Heliyon 10 (2024) e30279

Contents lists available at ScienceDirect

Heliyon

journal homepage: www.cell.com/heliyon

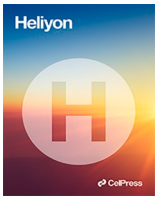

Research article

Study on the mechanism of magnesium calcium alloys/mineralized collagen composites mediating macrophage polarization to promote bone repair

Xiaojing Nie [a], Yonghua Shi [a], Lei Wang [b], Wumidan Abudureheman [a], Jingxin Yang [c], Chen Lin [a,*]

[a] Department of Pathology, School of Basic Medical Sciences, Xinjiang Medical University, Urumqi, Xinjiang, 830000, PR China
[b] School of Public Health, Xinjiang Medical University, Urumqi, Xinjiang, 830000, PR China
[c] Beijing Engineering Research Center of Smart Mechanical Innovation Design Service, Beijing Union University, No.4 Gongti North Road, Chaoyang District, Beijing, 100027, PR China

ARTICLE INFO

Keywords:
Magnesium-based metal
Osteogenic mechanism
Bone repair
Mineralized collagen

ABSTRACT

Magnesium-based composites are a focal point in biomaterials research. However, the rapid degradation rate of magnesium alloys does not align with the healing time of bone tissue. Additionally, the host reaction caused by magnesium implantation hampers its full osteogenic potential. To maintain an appropriate microenvironment, it is important to enhance both corrosion resistance and osteogenic activity of the magnesium matrix. In this study, a composite scaffold composed of mineralized collagen and magnesium alloy was utilized to investigate the regulatory effect of mineralized collagen on mouse macrophages and evaluate its impact on mouse bone marrow mesenchymal stem cells in terms of osteogenesis, immune response, and macrophage-induced osteogenic differentiation. This experiment examined the biocompatibility of mouse bone marrow mesenchymal stem cells and macrophage-induced osteogenic differentiation in vitro, and examined the expression levels of relevant pathways proteins. Magnesium calcium alloys/mineralized collagen exhibited extensive spreading, facilitated by broad and abundant pseudopodia that firmly adhered them to the material surface and promoted growth and pseudopodia formation. The findings revealed that magnesium calcium alloy/mineralized collagen scaffold materials induced osteogenic differentiation mainly through M2 polarization of macrophages. This effect was mainly mediated by promoting the integrin α2β1-FAK-ERK1/2 signaling pathways and inhibiting the RANK signaling pathways.

1. Introduction

With the increasing number of elderly individuals, there has been a significant rise in the prevalence of bone-related diseases worldwide [1]. Annually, over six million fractures occur globally, with 56 % requiring permanent or temporary internal fixation materials for surgical treatment [2,3]. Consequently, the development of biomaterials for internal fixation is an active area of research in orthopedics. Magnesium (Mg) and its alloys are biodegradable and good biocompatibility. Compared to other metals commonly

* Corresponding author.
E-mail address: linmao1977@xjmu.edu.cn (C. Lin).

https://doi.org/10.1016/j.heliyon.2024.e30279
Received 1 November 2023; Received in revised form 22 April 2024; Accepted 23 April 2024
Available online 26 April 2024
2405-8440/© 2024 The Authors. Published by Elsevier Ltd. This is an open access article under the CC BY-NC license (http://creativecommons.org/licenses/by-nc/4.0/).

used in clinical practice, Mg alloys have a similar modulus of elasticity to that of the bone cortex, thereby reducing the occurrence of the "stress shielding effect." However, degradability is advantageous for Mg alloys, but it also poses limitations as it can degrade rapidly without aligning with bone tissue healing time [4]. Moreover, host responses triggered by Mg alloy implantation hinder its full osteogenic potential. Therefore, one major limitation in traditional research lies in neglecting the significance of immune responses [5,6]. Timely and appropriate immune responses play a crucial role in promoting bone healing [7]. Henceforth, during synthesis techniques employed for Mg alloy composites fabrication, optimizing corrosion resistance within the Mg matrix and enhancing osteogenic activity become imperative to maintain an optimal "bone immune microenvironment." This will enable matching between matrix degradation rates and osteogenesis during in vivo implantation while addressing key challenges associated with clinical applications involving Mg-based metals. Several researchers have implemented this strategy within their studies on artificial bone grafting materials. Zeng and colleagues [8] prepared Mg–Li–1Ca with plasma electrolysis (MAO) coating and conducted experimental studies on its biocompatibility and corrosion resistance. They found that the coating of the MAO/PLLA composite materials greatly improved the corrosion resistance and compatibility of the cells. Mineralized collagen (nHAC) is a biomimetic composite material of nanohydroxyapatite and type I collagen. Bone, cartilage, sinews, and dentine are made of nHAC [9]. Therefore, nHAC can be used to repair bone defects, promote bone development, and accurately regulate bone immune responses. By regulating the polarization of macrophages during bone regeneration, nHAC can strongly induce enough M2 macrophages in vivo and in vitro to regulate the host immune response [10,11]. Regarding the regulatory role of bone biomaterials in osteogenesis, the immune response has both advantages and disadvantages. Adverse immune reactions can result in chronic inflammation and the formation of a fibrous capsule around the biomaterials, which hinders contact and integration between osteoblasts and the implant, thereby disrupting bone remodeling [12]. Therefore, we applied a coating of nHAC material to the surface of the Mg alloys. In our previous research, Mg^{2+}/Col I can stimulate the integrin α2β1-FAK-ERK1/2 pathway to promote osteogenesis [13]. RANK (NF-kB receptor activating Ligand) receptor activating ligand is a cytokine belonging to the tumor necrosis factor (TNF) family. It induces differentiation of precursor osteoclasts into mature osteoclasts. By activating corresponding signal transduction pathways, RANK stimulates differentiated osteoclasts to express specific genes that enable mature osteoclasts to undergo bone resorption and maintain their survival [14]. Hence, we investigated whether Mg–Ca/nHAC biomaterials promote osteogenic differentiation by regulating macrophage polarization and its underlying mechanisms. The aim of this study was to investigate the promotion of osteogenic differentiation by Mg–Ca/nHAC composite scaffolds through inducing macrophage polarization and the effect of scaffolds on mouse bone marrow mesenchymal stem cells (mBMSCs), so as to elucidate the mechanisms of Mg–Ca/nHAC composite scaffolds on bone repair.

2. Materials and methods

2.1. Preparation of materials

A magnesium-calcium (Mg–Ca) alloy sheet (with a calcium content of 1 wt%; 10 mm in diameter and 1 mm in height, weight 0.1245 g) was provided by Beijing Union University. The nHAC bone powder (supplied by Beijing Aojing Medical Technology Co., Ltd.) is an artificial bone repair material. Its nano-based apatite accounts for 45 % ± 5 %. It has a porosity range of 80–90 %, and pore sizes ranging from 50 to 500 nm. Preparation of Mg–Ca/nHAC: The nHAC solution (10 mg/mL in acetic acid) was evenly applied onto the surface of the Mg–Ca alloys.

2.2. Surface structure and characterization

We utilized the Oxford Quorum SC7620 Sputter Coating System to apply a gold coating (10 mA) for a duration of 45 s. Subsequently, the ZEISS GeminiSEM 300 scanning electron microscope was employed for sample observation, energy spectrum mapping, and other tests. The acceleration voltage was set at 3 kV during the recording of morphological characteristics. An SE2 secondary electron detector was utilized. Through this technique, we assessed the surface structure and element content distribution for each group of materials.

2.3. Materials degradation detection

In vitro degradation experiments were performed by accessing simulated body fluids (SBF). Concentrations of ions in SBF solution are similar to those in human plasma. The pH was adjusted to 7.4 and the temperature of the water bath was maintained at 37 °C. The materials were immersed in the SBF solution and placed in a 37 °C water bath using a 60 r/min speed. The degradation solution was changed every 24 h. The samples were washed with SBF, deionised water, dried, left at room temperature and then weighed. The main degradation products of Mg–Ca/nHAC are $Mg^{2+}$and Ca^{2+}. ICP-MS (Agilent 5110 OES, USA) was used to detect the concentration of Mg^{2+} and Ca^{2+}.

2.4. Osteogenic evaluation

2.4.1. Cell culture

According to the GB/T16886.5 standard, mouse bone marrow mesenchymal stem cells (mBMSCs, sourced from Shanghai Saibaikang) were added into DMEM supplemented with 10 mL/dL fetal bovine serum, 0.1 mol/L dexamethasone, 50 μg/mL Vitamin C, and 10 mmol/L β-sodiumglycerophosphate. The cells were cultivated in a constant temperature incubator (5 % CO_2, 37 °C).

2.4.2. Cell proliferation

The alloy was extracted using a complete culture medium at a concentration of 0.1 g/mL for 24 h. The Mg–Ca/nHAC sample was extracted at a ratio of 0.1 g/mL (Mg–Ca) and 60 mg/mL (nHAC). After filtration and sterilization, the experimental solution was divided into three groups: the control group, extraction solution to culture medium ratio of 1:2 group and extraction solution to culture medium ratio of 1:1 group. To collect mBMSCs at the logarithmic growth phase, cell counting was performed, and the cell concentration was adjusted to maintain a cell density of 1×10^4 cells/well in a 96-well plate. The cells were incubated at 37 °C with 5 % CO_2 for 24, 48, and 72 h. Following this, 100 μL of culture medium containing CCK-8 (Solarbio, China) was added to each well and incubated for 2 h in a constant temperature incubator at 37 °C. The absorbance was measured at 450 nm using an enzyme-linked immunosorbent assay.

2.4.3. Flow cytometry

The mBMSC cells in logarithmic growth phase were taken. Cell counted and cell concentration was adjusted. The cells were inoculated into 6-well culture plates at 1.5×10^5/well, 5 % CO_2, and incubated at 37 °C overnight to make the cells adherent to the wall. The experiment was divided into four groups: Control group, Mg–Ca group, nHAC group, and Mg–Ca/nHAC group. The cells were grouped according to the above treatment and cultured for 72 h. The cell suspension was transferred to a test tube and stained with 5 μL FITC/annexin V and 10 μL propidium iodide solution (Soraibao, China). The cells were gently vortexed and then incubated for 15 min at room temperature. Finally, 400 μL of Annexin V Binding Buffer was added to each tube and mixed evenly. The mixed solution was analyzed by flow cytometry.

2.4.4. Cell morphology analysis

The mBMSCs were seeded onto cover slides of different groups and placed in a 24-well plate (2 per well, 2×10^4 cells). The cells were grouped according to the above treatment and then cultured for 72 h. Control cover glasses treated with polylysine were used for comparison. Subsequently, 50 ng/mL PMA was added to the culture medium for 24 h to induce adherent cell formation. Following this, the cells were allowed to interact with the materials for one day. For SEM analysis, the sample was fixed in 3.7 % glutaraldehyde and observed using a scanning electron microscope (SEM) at a voltage of 3 kV after undergoing a graded ethanol dehydration series.

2.4.5. Cell adhesion

The mBMSCs were seeded into confocal dishes at a density of 6×10^4 cells/mL, with 1 mL of cell suspension per group and 3 replicate wells per group. After 7 days, the culture medium was removed, and the cells were fixed with 10 % paraformaldehyde for 10 min at room temperature. Subsequently, they were washed three times with PBS. A 0.5 % Triton X-100 solution was applied to allow the cells to permeabilize for 5 min. The cells were then incubated with 200 μL of TRITC-labelled phalloidin working solution (Solarbio, China) for 30 min at room temperature in the dark. The nuclei were stained with 200 μL of DAPI solution (Sorabio, China) for 30 s. Confocal microscopy was used to observe the cells and ImageJ software was employed to calculate cell areas.

2.5. Immunological evaluation

2.5.1. Cell culture

According to GB/T16886.5 standards, mouse macrophage RAW264.7 cells were provided by a company (Shanghai, China). The macrophages were cultured using DMEM culture medium.

2.5.2. Cell proliferation

The alloys were extracted using a complete culture medium at a concentration of 0.1 g/mL for 24 h, while the Mg–Ca/nHAC group was extracted at a ratio of 0.1 g/mL (Mg–Ca) and 60 mg/mL (nHAC). After filtering and sterilizing, the experimental groups were divided into three categories: the Control group, the groups with an extraction solution to culture medium ratio of 1:2, and the groups with an extraction solution to culture medium ratio of 1:1. The RAW264.7 cells were harvested during the logarithmic growth phase and then plated at a density of 1×10^4 cells/well in a 96-well plate. The cells were cultured at 37 °C in 5 % CO_2 for 24, 48, and 72 h. Following this, the culture medium was removed, and each well was washed three times with 100 μL PBS. Subsequently, each well was incubated with 100 μL of CCK-8 solution (Solarbio, China) at 37 °C for 2 h. The absorbance was measured at 450 nm.

2.5.3. Analysis of the morphology of macrophages

Macrophages were seeded onto cover slides of different grouping materials and placed in a 24-well plate (2 coverslips per well, with 2×10^4 cells each). A cover glass treated with polylysine served as the control. Next, 50 ng/mL PMA was added to the culture medium for 24 h to induce adherent cell formation. The cells were then allowed to interact with the material for one day. For SEM analysis, the sample was fixed in 3.7 % glutaraldehyde and observed in a graded ethanol series at a voltage of 3 kV using a scanning electron microscope (SEM).

2.5.4. Immunofluorescence staining

RAW264.7 macrophages were fixed on coverslips cultured with various materials using 4 % paraformaldehyde, permeabilized with 0.25 % Triton X, and blocked with 1 % BSA. Subsequently, IL-6 antibodies were diluted (1:100), applied to the coverslip, and allowed to incubate overnight at 4 °C. Coverslips were then exposed to secondary antibodies conjugated with either fluorescein isothiocyanate or tetramethyl rhodamine isothiocyanate for 30 min. Finally, the cells were stained with DAPI for 5 min to visualize the nuclei. The

Table 1
Primer sequences for RT-PCR analysis.

Target	Forward	Reverse
BMP-2	AAGCCAAACACAAACAGCGG	AAAGGCATGATAGCCCGGAG
ALP	AGCAGGTTTCTCTCTTGGGC	TGGGAGTCTCATCCTGAGCA
Runx-2	TCGTCAGACCGAGAAGTGGT	TTCAAGGTGCCGGGAGGTA
OCN	TCGTGTGTCTTCTCCACAGC	AGCCCTCTGCAGGTCATAGA
OPN	TGGCAGCTCAGAGGAGAAGA	TCTGTGGCGCAAGGAGATTC
VEGF	TCCGTAGTAGCCGTGGTCTGC	CCCTCTCCTCTTCCTTCTCTTCCTC
β-actin	CGATATCGCTGCGCTGGTC	AGGTGTGGTGCCAGATCTTC

samples were examined using a Zeiss laser scanning microscope (LSM510) equipped with LSM 5 release 4.2 software.

2.5.5. ELISA

The RAW264.7 macrophages were harvested for cell enumeration. A total of 2×10^5 cells per well were seeded in a six-well plate. Incubation was carried out at 37 °C with 5 % CO_2 for 72 h. Subsequently, they were cooled in a refrigerator at 4 °C for 30 min, followed by gentle agitation and collection. The cells were then washed with PBS, and the supernatant was discarded. The samples underwent two freeze-thaw cycles in liquid nitrogen. The protocol provided with the ELISA test kit (Elabscience) was adhered to for assaying the supernatants of macrophages cultured on diverse materials. We assessed the expression of M1-related cytokines including iNOS, IL-6, and CD80, as well as M2-related cytokines such as IL-10, Arginase-1 (Arg-1), and CD206.

2.6. Induction of osteogenic differentiation by macrophages

2.6.1. Cell culture

RAW264.7 cells were seeded in a 25 cm_2 cell culture flask with 4.0–5.0 mL of DMEM medium. They were cultured in a CO_2 incubator at 37 °C with a 5 % CO_2 concentration. The medium was refreshed every two to three days. For subculturing, cells were dissociated using 2.5 % trypsin. The collected supernatant was then transferred to cultured mBMSCs. A 1:1 mixture of macrophage medium and complete DMEM medium was used to cultivate mBMSCs. The culture medium was replenished every 2–3 days.

2.6.2. ALP (alkaline phosphatase) activity

The ALP activity of mBMSCs was assessed using the ALP kit (China Biyuntian Company). Cells were seeded into a 24-well plate at a concentration of 1×10^4 cells/mL, with 5 replicate wells per group. One milliliter of cell suspension was added to each well. After 7 days of incubation, the culture medium was aspirated and the cells were washed twice with PBS. Subsequently, 500 μL of 0.2 % (v/v) Triton X-100 (Sigma, USA) was added to the plate to lyse the cells. The ALP activity in the lysate was determined using the ALP kit. Finally, the optical density (OD) at 520 nm was measured using a spectrophotometer. The medium was discarded, the cells were washed twice with PBS, fixed with 4 % paraformaldehyde for 30 min, the fixative was discarded, stained according to the instructions of the alkaline phosphatase kit and the stained cells were photographed.

2.6.3. Real-time QPCR assay

The expression levels of osteogenic-related genes, including alkaline phosphatase (ALP), runt-related transcription factor 2 (Runx2), bone morphogenetic protein 2 (BMP-2), osteocalcin (OCN), osteopontin (OPN), and vascular endothelial growth factor (VEGF), were assessed via real-time PCR. Cells were seeded at a concentration of 1×10^5 cells/well and cultured for 7 days. Total RNA was extracted using Trizol (Ambion, USA). Subsequently, 1 μg of RNA from each sample was reverse transcribed into complementary DNA (cDNA) using the Prime ScriptTM RT reagent kit (Vazyme, USA). Table 1 provides the forward and reverse primers for the selected genes. Beta-actin was used as an internal reference. Data analysis was conducted using iQTM5 optical system software version 2.0.

2.6.4. Western blotting

The mBMSCs were cultured for 7 days in DMEM supplemented with 10 % fetal bovine serum. RIPA buffer (Beyotime, China) was employed for cell lysis. Protein concentration was determined using the BCA protein quantification kit (Beyotime, China). Subsequently, the protein sample was denatured by heating at 98 °C for 5 min and then loaded onto an SDS-PAGE gel. Following electrophoresis, the protein was transferred to a PVDF membrane. The membrane was then incubated with 5 % BSA for 2 h at room temperature, followed by washing with TBST. Primary antibodies including anti-FAK, anti-integrin α2, anti-integrin β1, RANK, and anti-ERK1/2 were applied, followed by overnight incubation at 4 °C. Subsequently, secondary antibodies were applied for 90 min. After washing with TBST, the membranes were treated with a chemiluminescence reagent and exposed. Immunoblotting images were semi-quantified using ImageJ.

3. Statistical analysis

In all experiments, a minimum of three samples per group were analyzed. One-way analysis of variance (ANOVA) was employed to assess differences between the two groups. Statistical significance between sample groups was determined. Quantitative data was

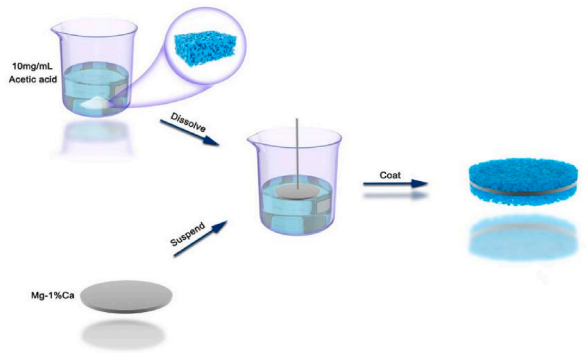

Fig. 1. The process of nHAC coated on the surface of Mg–Ca alloy.

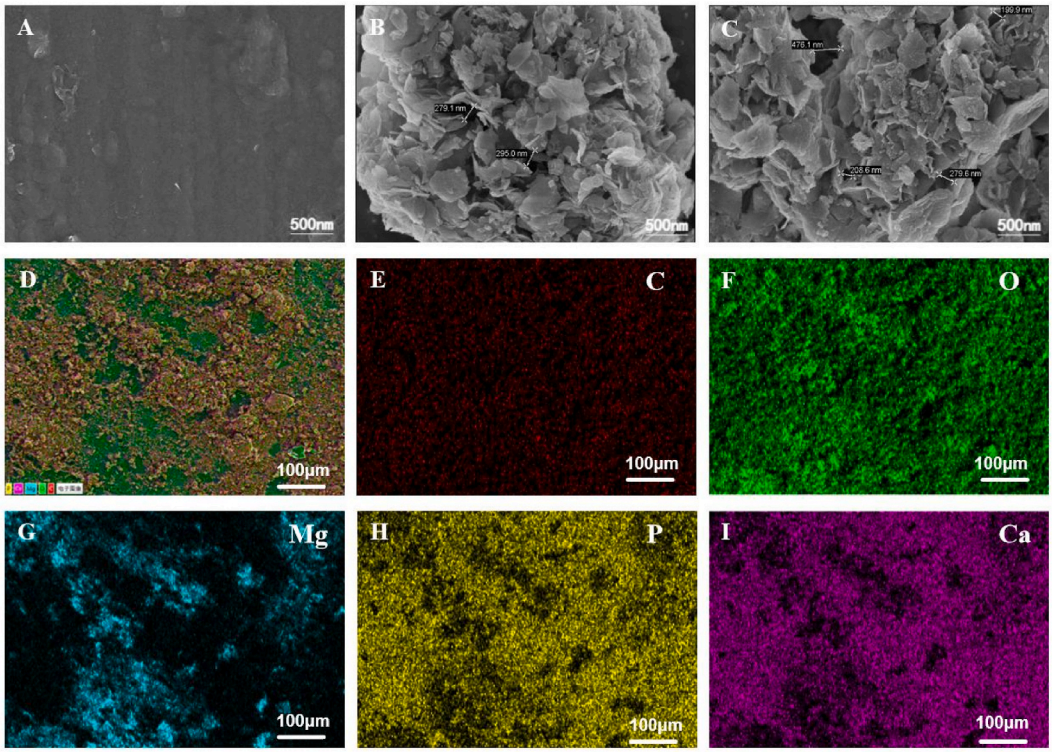

Fig. 2. **(A)** The surface of Mg alloys materials viewed under an SEM (scale bar: 500 nm). **(B)** The surface of nHAC materials viewed under an SEM (scale bar: 500 nm). **(C)** The surface of Mg–Ca/nHAC materials viewed under an SEM (scale bar: 500 nm). **(D-I)** The distribution of the content of the elements was observed by EDX spectra (scale bar: 100 μm).

represented as mean ± standard deviation for each group. Differences, both within and between groups, were considered statistically significant when $p < 0.05$.

4. Results

4.1. Preparation of materials

Preparation of Mg–Ca/nHAC: nHAC solution (10 mg/mL in acetic acid) was prepared and uniformly coated on the surface of Mg–Ca alloy (Fig. 1).

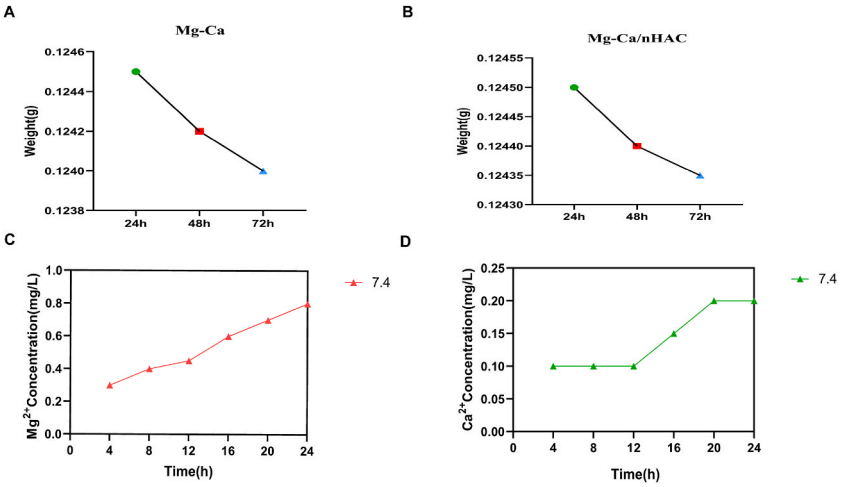

Fig. 3. **(A)** Changes in weight of Mg–Ca in SBF.·**(B)** Changes in weight of Mg–Ca/nHAC in SBF.·**(C)** Detection of Mg^{2+} concentration changes in Mg–Ca/nHAC materials using ICP-MS method. **(D)** Detection of Cg^{2+} concentration changes in Mg–Ca/nHAC materials using ICP-MS method.

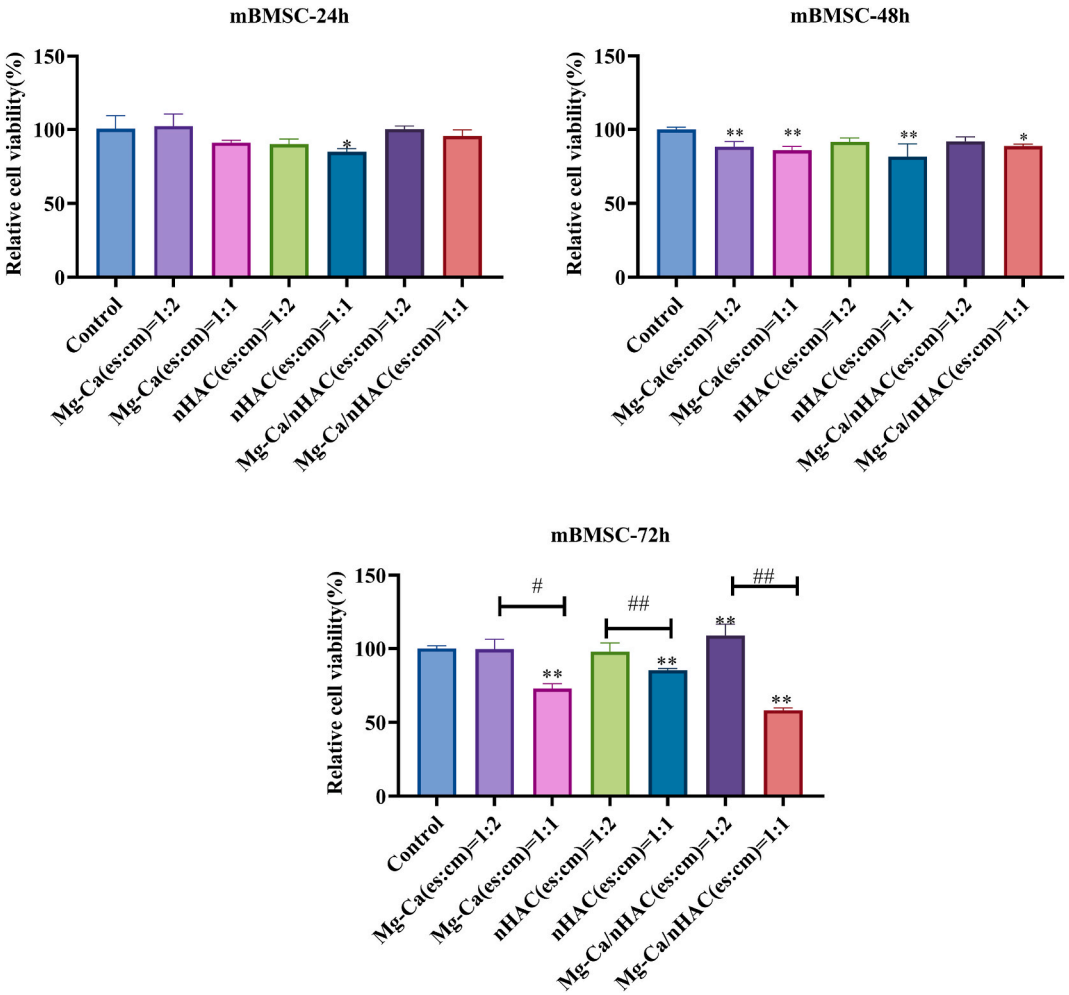

Fig. 4. Changes in cell viability of mBMSCs with samples for 24, 48, and 72 h (Compared to the Control group, *P < 0.05 and **P < 0.01); Comparison between groups, #P < 0.05 and ##P < 0.01; (Es: extraction solution; Cm: Culture medium).

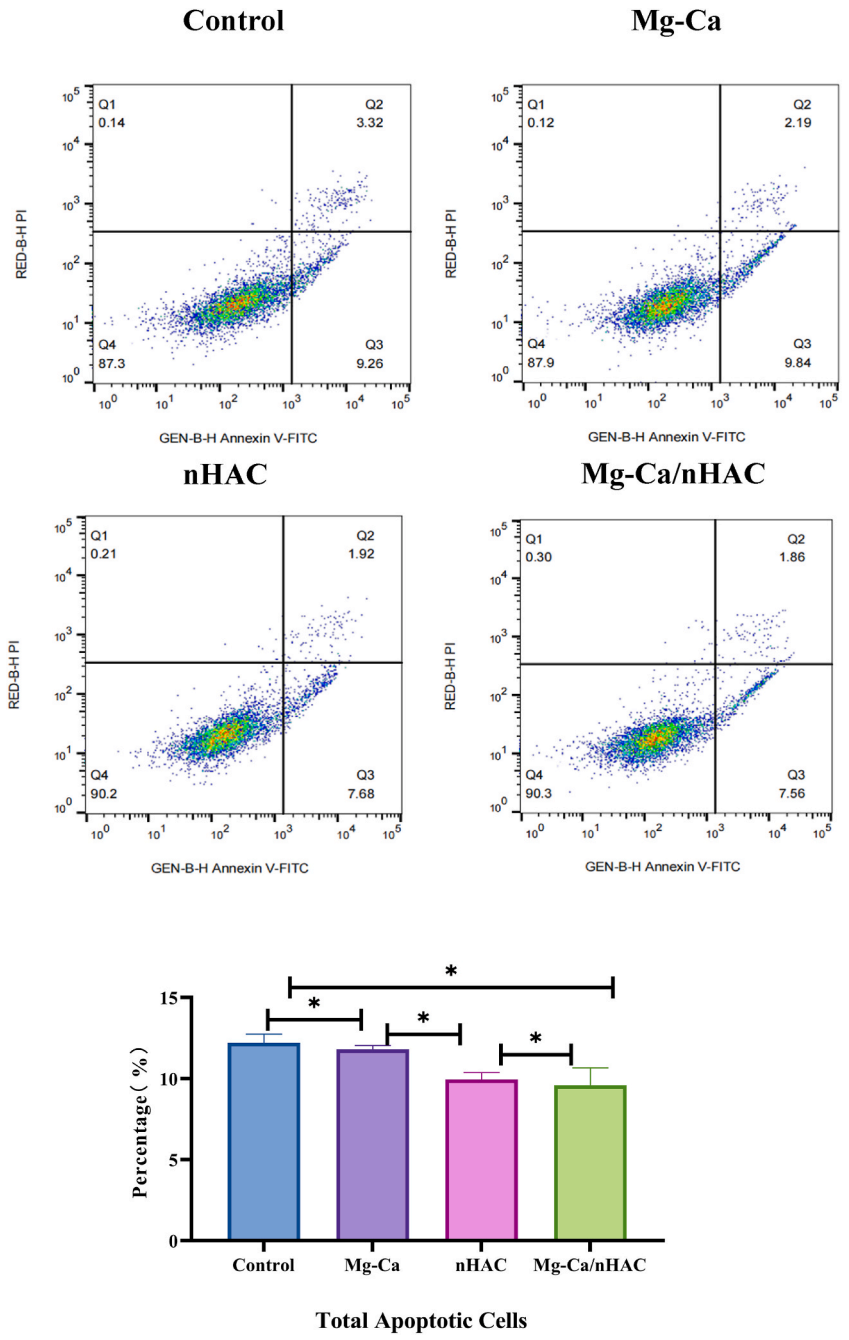

Fig. 5. Flow cytometer analysis results indicated that the total number of apoptotic cells in all three treatment groups were significantly lower compared to the control group. *p < 0.05.

4.2. Surface structure and characterization

The SEM micrographs of Mg–Ca, nHAC, Mg–Ca/nHAC were shown in Fig. 2. Fig. 2A showed the entire smooth surface and uniform microstructure of the Mg–Ca alloy, at the same time, a slight oxidation can be found on the surface. Fig. 2B showed that the nHAC layer is a three-dimensional nanoscale structure that presents a sheet-like structure of disordered growth outward, forming a pore structure on the surface, paving the way for cells to be implanted from the outside. Fig. 2C showed the three-dimensional nanoscale nHAC of the Mg–Ca/nHAC group growing on the surface of the Mg–Ca alloy. Most of the pores in nHAC nanostructures are interconnected, facilitating cell adhesion and growth. EDX spectra of Mg–Ca/nHAC composite coatings show the presence of Ca, Mg, P, and O (Fig. 2D–I). The high oxygen content may be the cause of sample oxidation. Because nHAC contains nano-hydroxyapatite, it is rich in

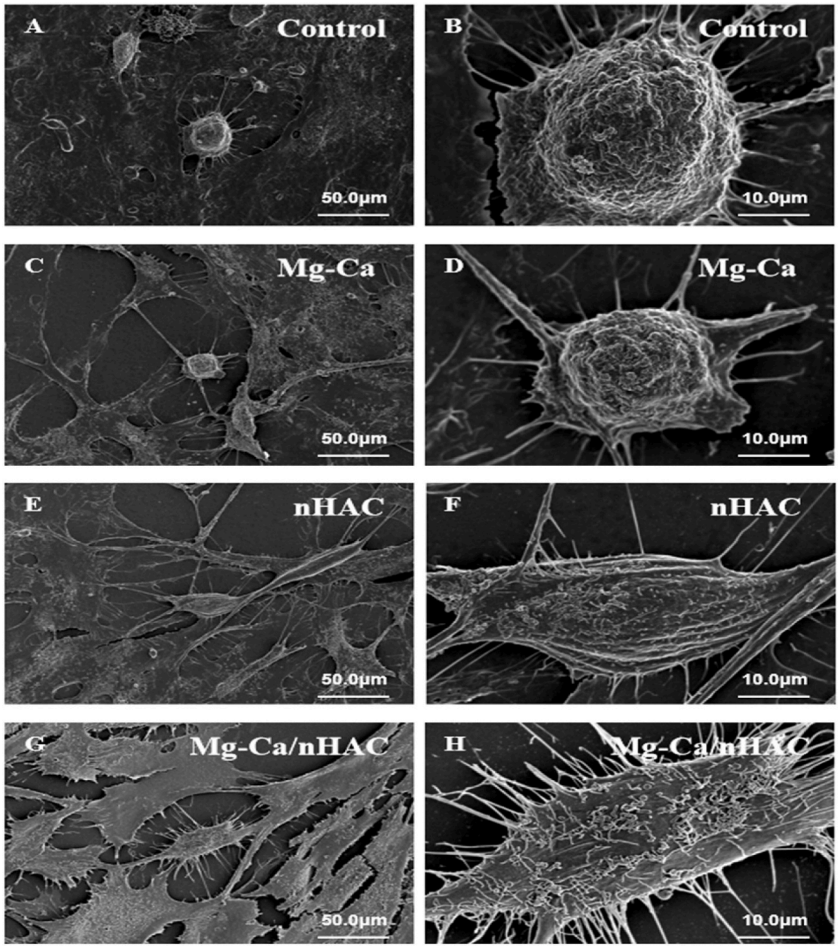

Fig. 6. SEM images of the morphological characteristics of mBMSCs after treatment with different materials (scale bar: 50 μm and 10 μm).

calcium, phosphorus and other elements.

4.3. Materials degradation detection

The degradation experiments of Mg–Ca and Mg–Ca/nHAC materials were tested in SBF respectively and Fig. 3A showed that Mg–Ca alloys had a relatively fast degradation rate in 24–48 h and the rate of degradation became slow after 48 h. Fig. 3B showed that the Mg–Ca/nHAC materials are the same as above. However, comparing the two groups of materials, the degradation rate of Mg–Ca/nHAC materials were slower. This indicated that the nHAC coatings were beneficial to reduce the degradation rate of Mg–Ca alloys. Fig. 3C showed that the concentration of Mg^{2+} gradually increased over time. However, there was no significant changes in the concentration of Cg^{2+} during the 12 h. During 12–20 h, the concentration showed an upward trend over time. After 20 h, the concentration did not change significantly and remained stable (as shown in Fig. 3D).

4.4. Osteogenic evaluation

4.4.1. Cell proliferation

Initially, we used the CCK-8 kit (Fig. 4) to assess the growth of mBMSCs. The experimental groups consisted of a control, as well as groups with extract-to-medium ratios of 1:2 and 1:1. Each treatment was repeated three times. The results showed that at 24 h, there was no significant difference in the proliferation of mBMSCs between the treatment and control groups. Only a slight reduction in cell viability was observed when the collagen extract-to-medium ratio was 1:1, although the difference was not substantial.

However, as the treatment duration extended to 48 and 72 h, noticeable discrepancies in mBMSC viability emerged between the treatment groups and the control group. The highest level of cell activity was observed when the extract-to-medium ratio was 1:2. Consequently, for subsequent experiments involving mBMSCs, we opted for a 1:2 ratio of extract solution to medium.

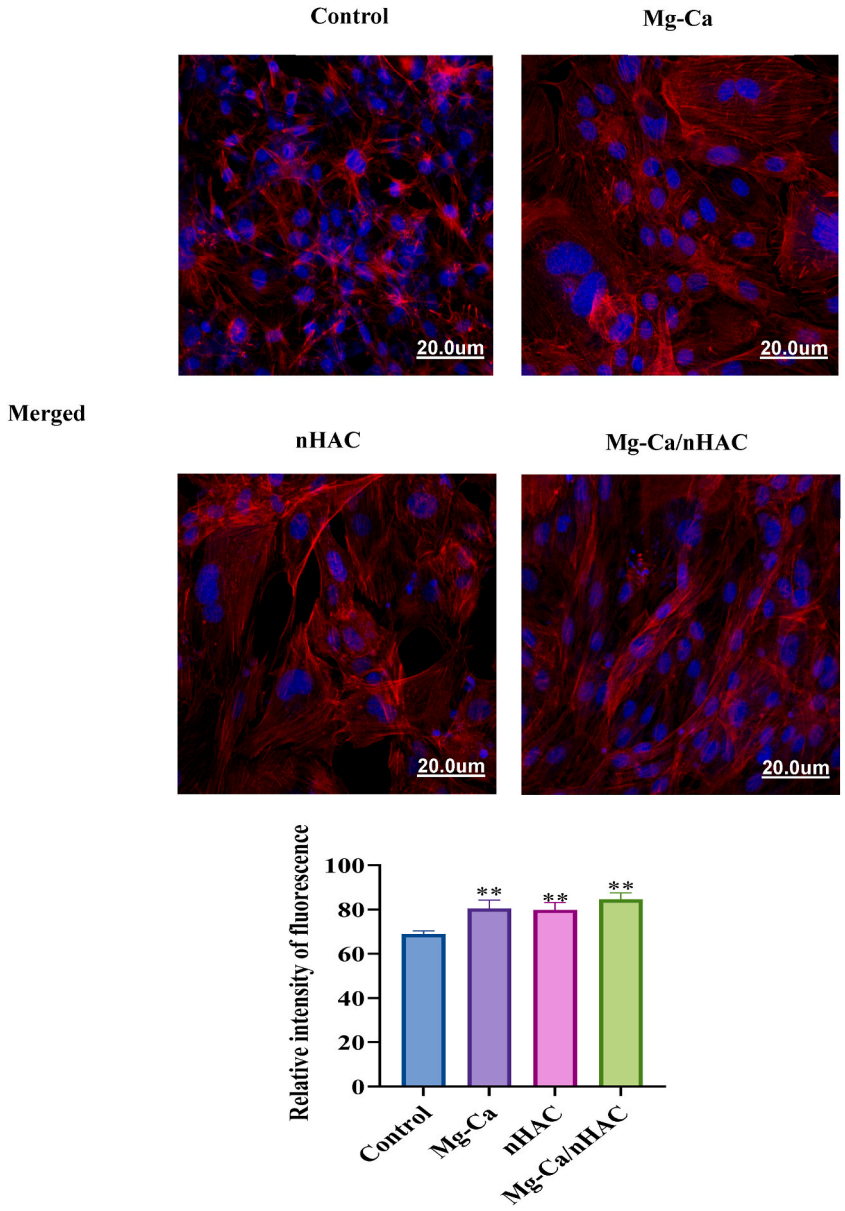

Fig. 7. The morphology of mBMSCs cultured with samples for seven days was analyzed by confocal microscopy (scale bar: 20 μm). Actin filaments were shown red was and the nucleus were shown blue. One-way ANOVA (n = 3 per treatment group). **p < 0.01 vs. control group.

4.4.2. Flow cytometry

Flow cytometry was employed to assess changes in cell apoptosis using GRN-B and RED-B channels. As depicted in Fig. 5, the results indicated that the total number of apoptotic cells in all three treatment groups were significantly lower compared to the control group. Additionally, both Mg–Ca and nHAC demonstrated a positive impact on cell growth. Notably, the significant enhancement of cell growth observed after Mg–Ca/nHAC treatment showed a significant difference between the two groups.

Furthermore, the total number of apoptotic cells in the Mg–Ca/nHAC group was significantly reduced compared to both the nHAC and control groups. Among the three experimental groups, the Mg–Ca/nHAC group exhibited the lowest number of apoptotic cells, suggesting a significant positive impact on cell growth.

4.4.3. Cell morphology analysis

The impact of different materials on the morphology of mBMSCs was investigated by studying their morphological changes using scanning electron microscopy (SEM) after inoculation and culturing on various surfaces. The SEM analysis results are depicted in Fig. 6. The observations revealed distinct morphological characteristics for each group. Compared to the blank group, cells show more obvious stretching and expansion in Mg–Ca group. Although their cell bodies remained spherical and not entirely elongated. In the

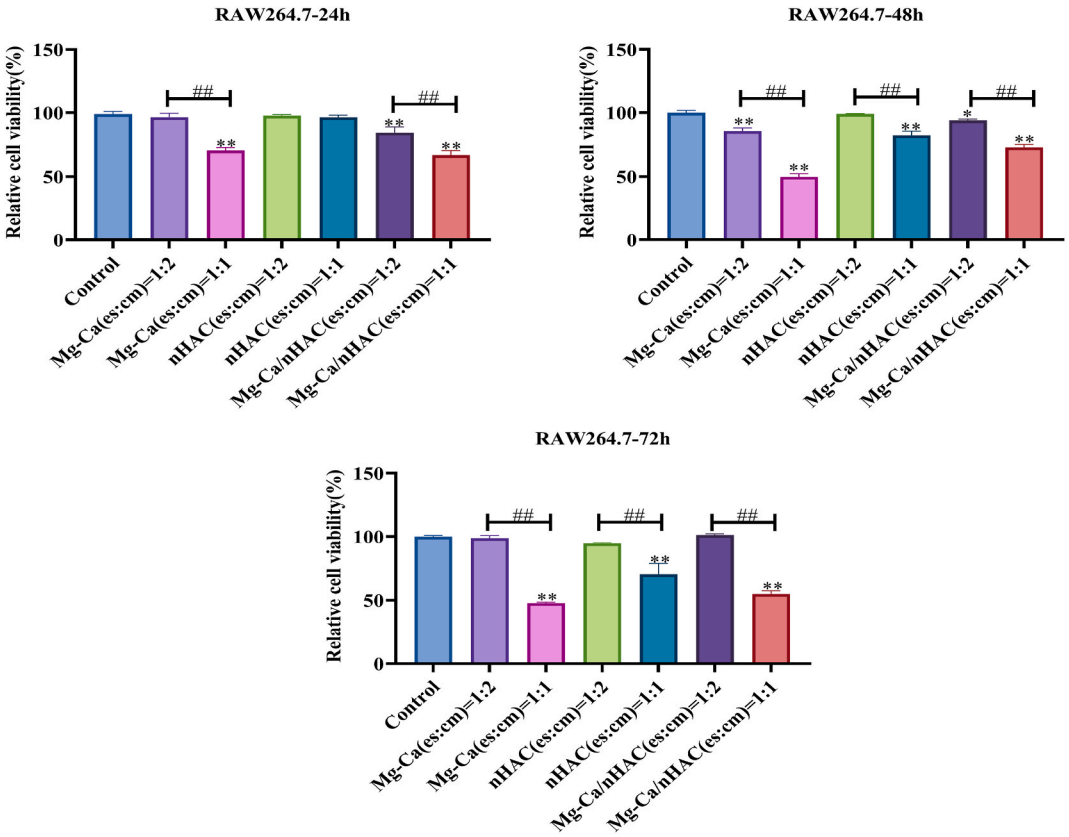

Fig. 8. Changes in the viability of RAW264.7 cells with samples for 24, 48, and 72 h (Compared to the Control group, *P < 0.05 and **P < 0.01); (Comparison between groups, #P < 0.05 and ##P < 0.01); (Es: extraction solution; Cm: culture medium).

nHAC group, cells also exhibited expansion, and pseudopodia were discernible, albeit in lower numbers. Conversely, cells exhibited full expansion and flattened outward in the Mg–Ca/nHAC group. The presence of wide and numerous pseudopodia facilitated cell adhesion to the material's surface, promoting the growth and development of pseudopodia. These findings corroborate earlier research, highlighting that Mg–Ca/nHAC treatment was the most effective in promoting cell adhesion and cell growth, followed by nHAC and Mg–Ca treatments.

4.4.4. Cell adhesion

F-Actin (Phalloidin) staining was utilized to investigate the cytoskeleton. Confocal microscopy was used to observe the cells. Image J software was used to quantify areas. The observed alterations in cell morphology corresponded with those depicted in the SEM images. In the control group (Fig. 7), cells exhibited a flattened and minimally extended appearance. Conversely, cells in the Mg–Ca group, nHAC group, and Mg–Ca/nHAC group displayed a widespread distribution. Additionally, these cells appeared elongated and stretched, and their actin filaments were distinctly discernible. Although there were no significant differences between groups. Notably, cells in the Mg–Ca/nHAC group exhibited a good dispersed appearance. It is suggested that Mg–Ca, nHAC, Mg–Ca/nHAC composite scaffolds enhanced cell adhesion and growth, which is beneficial for promoting osteogenic differentiation and bone repair.

4.5. Immunological evaluation

4.5.1. Cell proliferation

The experimental group was divided into three subgroups (Fig. 8): the Control group, groups with an extraction solution to culture medium ratio of 1:2, and groups with an extraction solution to culture medium ratio of 1:1; each treatment subgroup was subjected to three replicate wells. The results revealed that after 24 h, when the ratio of extraction solution to culture medium was 1:1, the viability of cells in the Mg–Ca group and the Mg–Ca/nHAC group significantly decreased. However, compared to the cells in the control group, those in the nHAC group exhibited no significant difference in viability.

At 48 h, with the extraction solution to culture medium ratio set at 1:1 across the three groups, cell viability was notably lower compared to the other groups. This trend was the same at 72 h, with the same 1:1 ratio yielding lower cell viability in these groups. Treatment with an extraction solution to culture medium ratio of 1:2 significantly enhanced cell viability across all three treatment groups, aligning with the findings presented in Fig. 4.

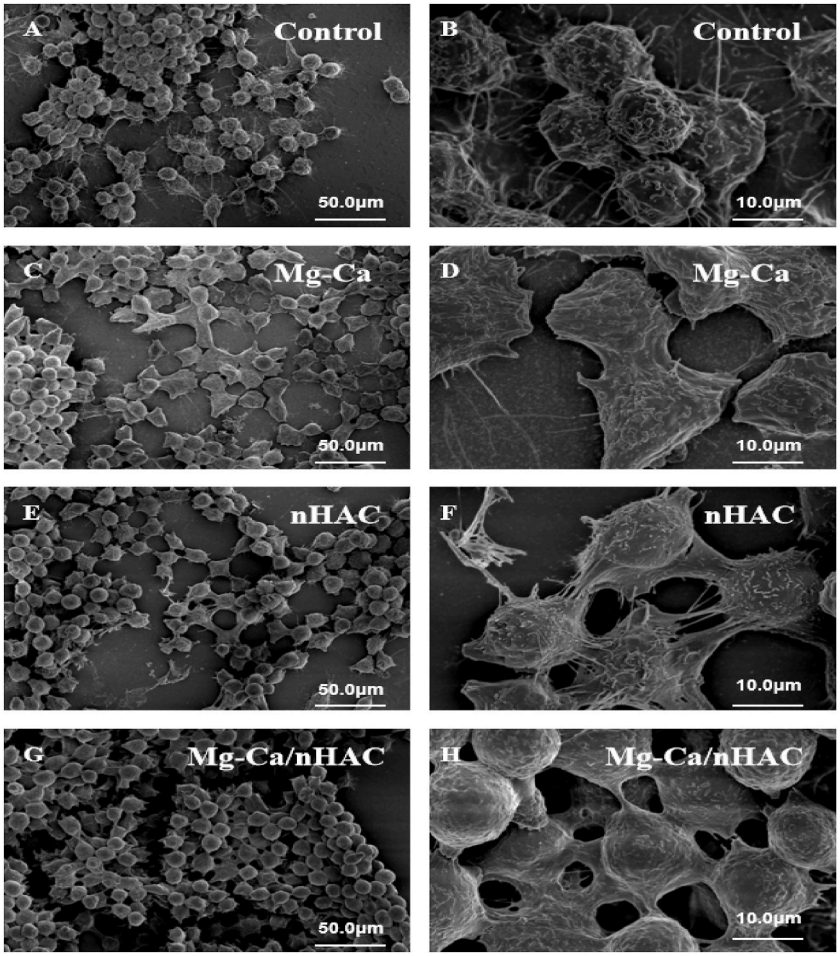

Fig. 9. Scanning electron microscopy images of the morphology of macrophages in different material treatment groups (scale bar: 50 μm and 10 μm).

Both mBMSCs and RAW264.7 cells exhibited the most substantial inhibition of proliferation when exposed to an extract ratio of 1:1. Conversely, cell activity reached its peak when the extract-to-culture medium ratio was set at 1:2. Consequently, we employed a 1:2 ratio of extraction solution to culture medium for treating RAW264.7 cells in subsequent experiments. These results suggest that varying concentrations of degradation product components exert differential effects on cell behavior over time.

4.5.2. Analysis of the morphology of macrophages

To assess the influence of different materials on macrophage morphology, macrophages were seeded and cultured on various surfaces. Morphological alterations in macrophages were examined using scanning electron microscopy, and the corresponding SEM images are presented in Fig. 9. The findings revealed distinct morphological features in each group.

In the Mg–Ca group, cells exhibited elongation, although their pseudopodial extensions were not fully pronounced compared to cells in the control group. Cells in the nHAC group also displayed elongation, with relatively fewer pseudopodia extending. These pseudopodia assumed a radiating sun rays pattern, predominantly indicative of the classic M1 phenotype. Conversely, cells in the Mg–Ca/nHAC group had spherical cell bodies extending towards the poles, resembling the typical M2 phenotype. The cell density in this group was akin to that of the M2 phenotype. The extensive pseudopodia firmly anchored the cells to the material's surface. This observation aligns with earlier results, emphasizing that Mg–Ca/nHAC treatment was more conducive to cell adhesion and growth.

4.5.3. Immunofluorescence staining

The experimental findings are presented in Fig. 10. Quantification of fluorescence areas using Image J software. Compared with the control group, the fluorescence intensity of IL-6 was reduced in the Mg–Ca group, nHAC and Mg–Ca/nHAC group and it was statistically significant in the nHAC and Mg–Ca/nHAC group (**$P < 0.01$). Comparisons between groups were statistically different in the Mg–Ca and nHAC groups, Mg–Ca/nHAC group (***$P < 0.001$). Whereas, in the experimentally treated group, The results showed that nHAC and Mg–Ca/nHAC had significant anti-inflammatory effects and favoured macrophage polarization towards the M2 phenotype.

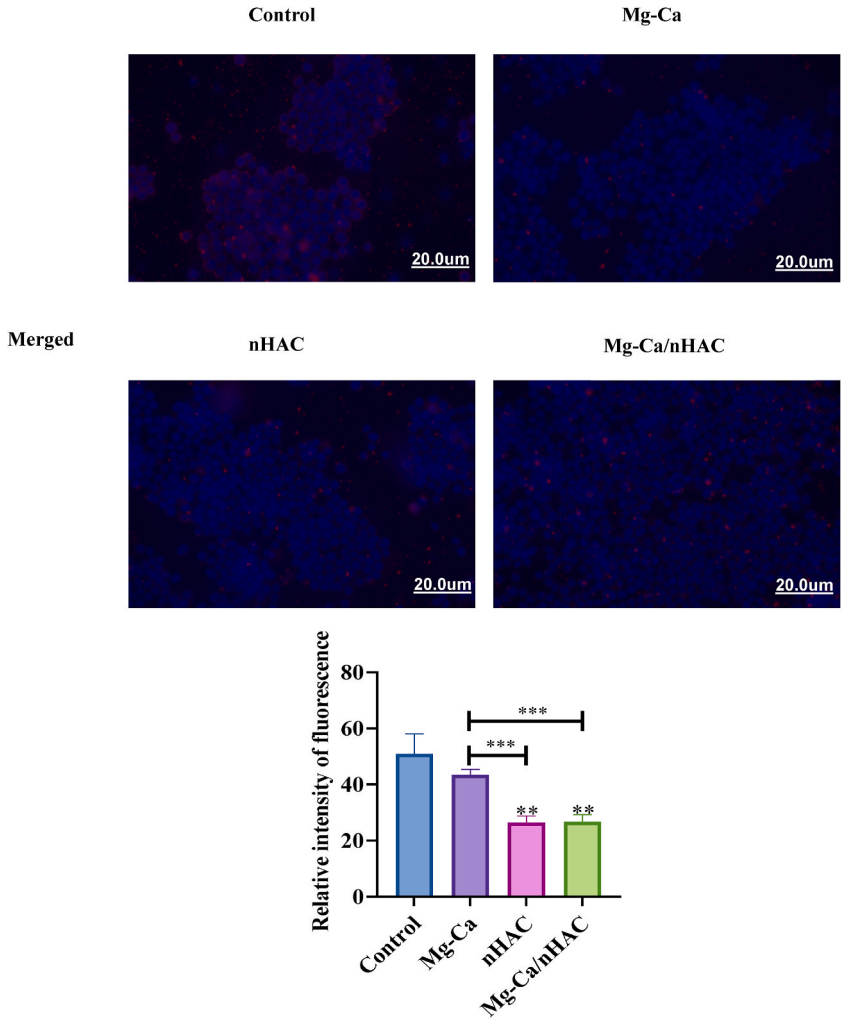

Fig. 10. The luminescence of IL-6 in cells was observed under an inverted fluorescence microscope (scale bar: 20 μm). One-way ANOVA (n = 3 per treatment group). **p < 0.01 vs. control group and ***p < 0.001.

4.5.4. ELISA

Macrophage supernatants cultured with different materials were subjected to ELISA according to instructions. The secretion of M1-related cytokines, namely iNOS, IL-6, and CD80, as well as M2-related cytokines, IL-10, arginase-1 (Arg–1), and CD206, were assessed. The ELISA results demonstrated a significant upregulation of some markers associated with mouse M2 macrophages (IL-10, Arg–1, and CD206) in the mineralized collagen group compared to the control group. In the Mg–Ca/nHAC group, the expression of M2 markers (Arg–1 and CD206) was higher, while the M1 marker (IL-6) significantly decreased compared to the control group. The results of this experiment are consistent with the results of macrophage morphology analyses. These findings suggest that Mg–Ca/nHAC composite scaffolds promote macrophage polarization in the M2 direction. The expression of iNOS and CD80 also decreased, though the extent of change was less prominent, indicating that Mg–Ca/nHAC composite scaffolds may modulate macrophage polarization (Fig. 11).

4.6. Induction of osteogenic differentiation by macrophages

4.6.1. Alkaline phosphatase activity

We investigated the impact of macrophage polarization on the osteogenic differentiation of bone marrow mesenchymal stem cells through an ALP activity assay, with results depicted in Fig. 12. Perform the ELISA according to the ALP assay kit instructions. Calculation was performed using the designated formula and the data was plotted using GraphPad Prism. The ALP activity of the Mg–Ca/nHAC group recorded the highest value. Moreover, both the Mg–Ca alloy group and Mg–Ca/nHAC group exhibited higher ALP activity compared to the control group. Both Mg–Ca, nHAC, and Mg–Ca/nHAC composite scaffolds significantly enhanced ALP activity. Moreover, the ALP activity in the Mg–Ca/nHAC group significantly surpassed that of all other groups. Photography under a light microscope, noticeable distinctions in blue nodules were observed across various treatment groups, particularly in the Mg–Ca/nHAC

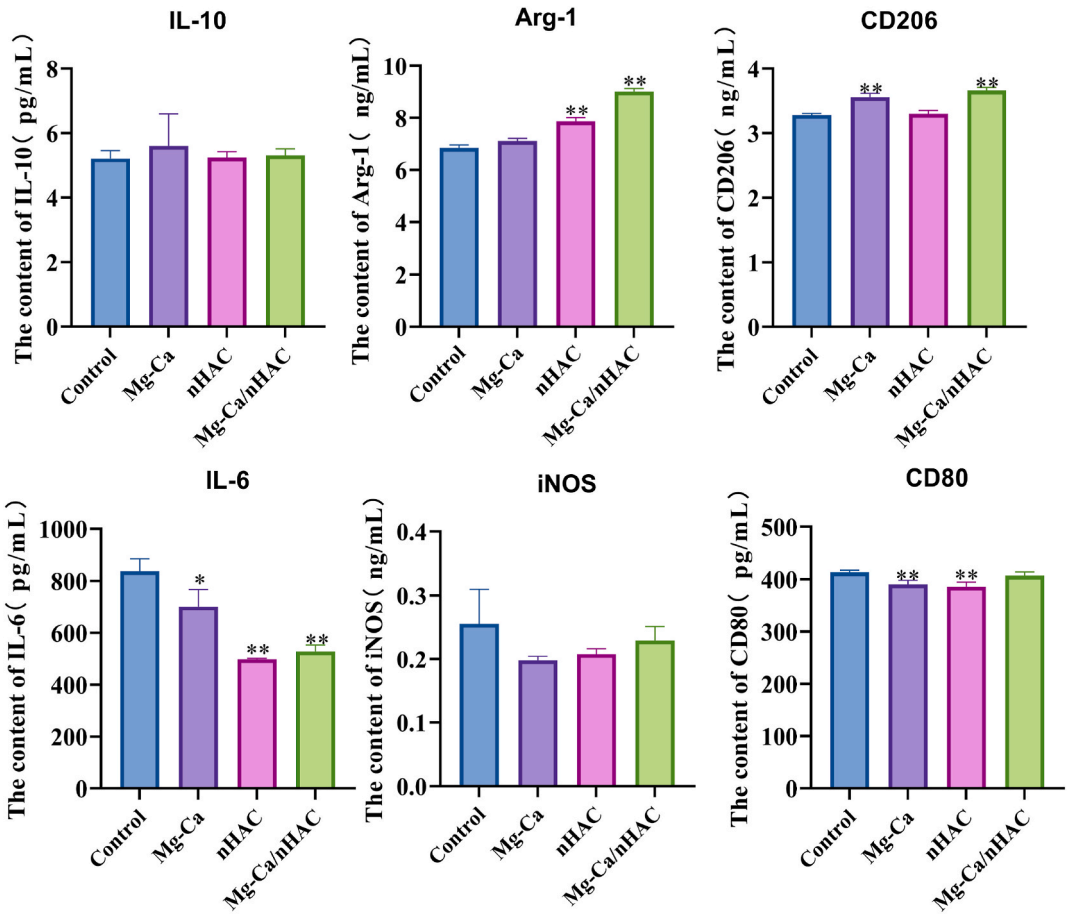

Fig. 11. Changes in the content of various indicators in cell lysate after they were co-cultured with RAW264.7 cells and different experimental treatment groups for 72 h; *p < 0.05 vs. control group and **p < 0.01 vs. control group.

group. Positively stained cells appeared as dark bluish-purple.

4.6.2. Expression of osteogenic genes

To assess whether macrophage polarization enhances osteogenesis, we collected macrophage supernatant for culturing mBMSCs and subsequently determined the expression levels of osteogenesis-related genes (OPN, OCN, ALP, RUNX2, BMP-2, and VEGF) using RT-qPCR. The results revealed a significant increase in the expression of osteogenic genes in the Mg–Ca group, nHAC group, and especially in the Mg–Ca/nHAC group compared with the control group. These findings strongly suggested that macrophage polarization had a notable influence on the osteogenic differentiation of mBMSCs.

Moreover, the expression level of osteogenic genes in Mg–Ca/nHAC composite scaffolds were significantly upregulated, indicating the potential of Mg–Ca/nHAC to promote the osteogenic differentiation of mBMSCs by modulating macrophage polarization (Fig. 13). The ELISA resulted also supported this observation, demonstrating that macrophages polarized toward the M2 phenotype exerted a positive influence on osteogenic differentiation.

4.6.3. Western blotting

Expanding on our previous discoveries, we aimed to explore its potential in upregulating the integrin α2β1-FAK-ERK1/2 pathway, while concurrently suppressing the RANK pathway, with the ultimate goal of promoting osteogenesis. Protein levels of FAK, α2, β1, ERK1/2, and RANK were evaluated through Western blot assays. The results showed significantly enhanced expression of integrin α2 and ERK1/2 proteins in the Mg–Ca/nHAC group compared with the other groups. In contrast, the expression levels of FAK and RANK proteins were significantly lower (as shown in Fig. 14).

5. Discussion

In recent years, the role of Mg alloys as bone repair materials has been widely scrutinized in research. However, the rapid degradation of Mg alloys presents a challenge, as it may not align with the required healing time for bone tissue. Additionally, the

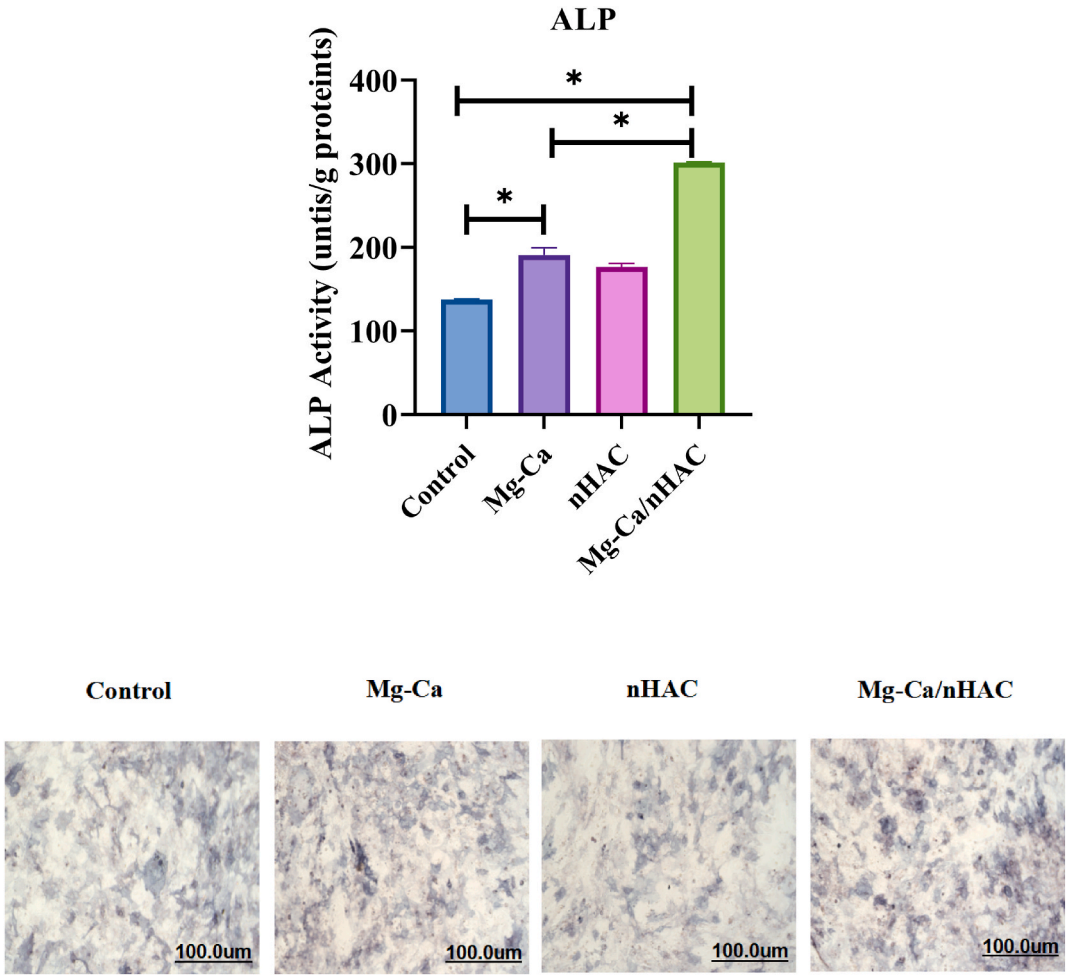

Fig. 12. After the samples were cultured with mBMSCs for 7 days, ALP activity of the samples was measured and photographed (scale bar: 100 μm). *p < 0.05.

accelerated degradation and formation of hydrogen gas may impact the host organism's response. To address these limitations, researchers have successfully employed surface coatings or alloys to modify their physical and chemical properties [15–17]. Mg–Ca ternary or Zn alloyodegradable alloys composed of Mg, zinc, and calcium have gained attention in recent years [18–20]. Therefore, we used nHAC solution (10 mg/mL acetic acid solution) uniformly applied to the surface of Mg–Ca alloys to detect the degradation rate. As shown in Fig. 3A-B, the corrosion resistance of Mg–Ca alloys were enhanced by nHAC coating. Furthermore, the porous 3D structure of mineralized collagen has a high capacity to bind serum proteins and absorb calcium ions, which may be beneficial in promoting cell attachment, growth and differentiation [21–23]. Bone immune microenvironment plays a key role in bone regeneration process. Among various players, innate immune cells such as macrophages play a crucial role [24,25]. Some studies have found that Mg alloys stimulate inflammation. However, on the 5th and 10th day post implantation, Mg alloys exhibited significant regulatory effects on macrophage polarization towards the M2 type. This process subsequently promotes tissue healing while reducing immune responses to degradation products from the alloy. These effects are attributed to ions (Mg, Zn, and Ca ions) released during early surface degradation interacting with intracellular ion channels. Firstly, we constructed composite scaffolds and then this experiment used scanning electron microscope and energy spectrum mapping to observe the surface morphology and elemental distribution of each group of material scaffolds, and found that a large number of uniform pores existed on the surface of all porous scaffolds, which may be caused by the presence of nHAC powder in the form of aggregates on the surface of the materials (as shown in Fig. 2B and C). The materials surface had a certain porosity. The porosity of bone tissue engineering scaffolds is essential for promoting endogenous cell migration and inward growth of newborn bone. When porous scaffolds are used for bone tissue engineering, the presence of pore structure promotes cell spreading and intercellular transport and facilitates cell adhesion and growth [26,27]. As shown in Fig. 2D-I, EDX spectra of Mg–Ca/nHAC composite scaffolds show the presence of Ca, Mg, P, and O. The high oxygen content may be the cause of sample oxidation. Because nHAC contains nano-hydroxyapatite, it is rich in calcium, phosphorus and other elements. Therefore, we conducted experiments in vitro to investigate the role and mechanism of Mg–Ca/nHAC scaffolds in promoting the biological behaviour of mBMSCs by regulating the bone immune microenvironment. The results of the CCK8 experiment (shown in Figs. 4 and 8) indicated

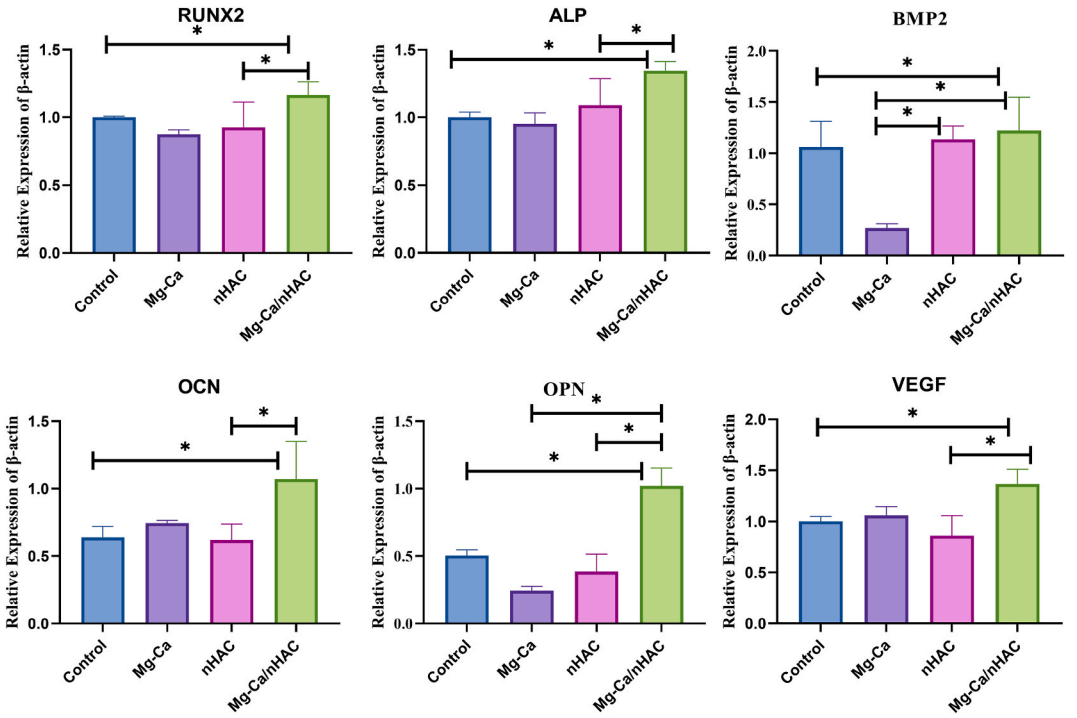

Fig. 13. The level of expression of the osteogenesis-related genes RUNX2, ALP, BMP2, OCN, OPN and VEGF after 7 days of treatment were quantified by PCR.*$p < 0.05$.

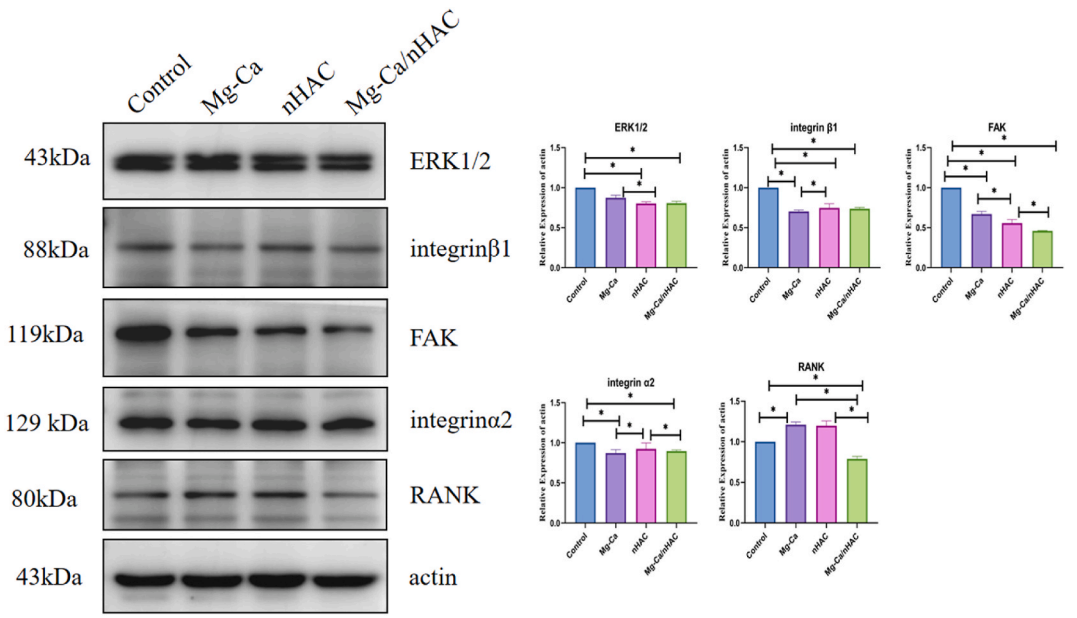

Fig. 14. After seven days of incubation, the levels of expression of FAK, integrin α2, integrin β1, ERK1/2, and RANK were compared. *$p < 0.05$.

that there was no significant difference observed in RAW264.7 cells when the extract vs media ratio was 1:1. Treatment of mBMSCs, at 24, 48 h, there was no significant difference in cell viability between the groups, while at 72 h, both the Mg–Ca and nHAC groups had a significant promotion of cell viability when the ratio of the extract to the medium was 1:2. It is noteworthy that the cell viability was significantly increased when the ratio of extract to medium was 1:2 in the Mg–Ca/nHAC group. While when the ratio of extract to medium was 1:1, there was a significant inhibition of cell viability, which suggests that the Mg–Ca and nHAC groups have a synergistic effect. It may also be due to the different effects of different concentrations of Mg^{2+} and nHAC on cells behaviour. Wang et al. showed

that 6–10 mM Mg^{2+} promoted adhesion and proliferation of osteoblasts. Among them, 10 mM Mg^{2+} significantly promoted the adhesion and differentiation of osteoblasts, and 18 mM Mg^{2+} significantly inhibited the proliferation and differentiation of osteoblasts [28]. Based on the results of CCK8 experiments and related literatures, it was shown that the Mg^{2+} concentration of the Mg–Ca/nHAC group was in the range of 10 mM at a 1:2 ratio of extract to medium, while the Mg^{2+} concentration of the Mg–Ca/nHAC group was greater than or equal to 18 mM at a 1:1 ratio of extract to medium. So based on the results above, we treated the cells with a 1:2 ratio of extract to medium in order to determine the compatibility of different materials with mBMSCs through cell apoptosis and cell adhesion, cell morphology analysis. As shown in Fig. 4, the experimental results showed that compared to the control group, the experimental treatments significantly inhibited apoptosis, especially the Mg–Ca/nHAC group had the strongest ability to inhibit apoptosis, followed by the nHAC group. The comparison between groups was also statistically significant. nHAC group had a greater ability to inhibit apoptosis than Mg–Ca group. The results of apoptosis experiments showed a significant reduction of apoptotic cells in the Mg–Ca/nHAC group, indicating better biocompatibility. It was also consistent with the results of CCK8 experiments. As shown in Fig. 6, compared to the control group, cells within the Mg–Ca/nHAC group exhibited full extension and flattening towards their surroundings, with broad and abundant pseudopodia firmly anchoring them to the material surface. This promoted cell growth and increased pseudopod count. The results indicated that the Mg–Ca/nHAC group had superior efficacy in promoting osteogenic differentiation, followed by the nHAC group and then the Mg–Ca group. Cells in contact with materials usually undergo three stages: adhesion, proliferation and differentiation. The state of cell adhesion directly affects the subsequent proliferation and differentiation of cells [29]. The results of the experiments are shown in Fig. 7. These cells appeared elongated and stretched, and their actin filaments were clearly visible. The cells in the Mg–Ca/nHAC group showed a particularly dispersed appearance, suggesting that the Mg–Ca/nHAC composite scaffolds are favourable for cell adhesion, further also promoting cell proliferation and differentiation. The bone immune microenvironment plays an important role in promoting osteogenesis, in order to verify whether the material scaffolds play an osteogenic role through the bone immune microenvironment. Morphological analysis and ELISA were performed on RAW264.7 macrophages (Fig. 9). The Mg–Ca/nHAC group displayed higher cell density, enhanced growth state, and more extended synapses compared to other groups. Cells within this group exhibited elongation towards poles-characteristic features of M2 phenotype [30]. Macrophages are innate immune cells that play an important role in substance-induced immune responses. Biomaterial implantation can induce the polarization of macrophages to M1 and M2 phenotypes. M1-type macrophages are mainly activated by Th1-type cytokines and show high expression of MHCII, produce large amounts of TNF-α, IL-12 and NO. M1-phenotype macrophages are associated with the release of pro-inflammatory cytokines such as IL-1β, TNF-α and IL-6. M2-type macrophages are mainly activated by Th2-type cytokines, which are mainly expressed as CD206, and through the secretion of the inhibitory cytokine IL-10. M2-type macrophages are associated with anti-inflammatory responses and tumour diseases [31,32]. As shown in Fig. 11, ELISA results showed significant up-regulation of certain markers associated with M2 macrophages (IL-10, Arg-1, CD206) in comparison to the control group for Mg–Ca/nHAC treatment. Moreover, we further detected IL-6 by immunofluorescence staining experiments, which showed that in the control group, the fluorescence intensity of IL-6 was significantly higher, while in the experimentally treated group, the fluorescence intensity of IL-6 was significantly lower (as shown in Fig. 10). This observation suggests that Mg–Ca/nHAC has a significant anti-inflammatory effect, which is conducive to promoting its polarization towards the M2 phenotype. Based on these results, we conjectured whether Mg–Ca/nHAC promotes osteogenic differentiation of mBMSCs by modulating macrophage polarization towards the M2 phenotype, which facilitates bone repair. Macrophage supernatants were collected and added to the medium to treat mBMSCs. The expression levels of osteogenic markers (OPN, OCN, ALP, RUNX2, BMP-2, and VEGF) were assessed by RT-qPCR and ALP activity assay. Notably, ALP is a crucial indicator for osteoblast differentiation. The results obtained from the ALP experiments (Fig. 12) demonstrated that the Mg–Ca/nHAC group exhibited significantly higher ALP activity with dark blue-purple positive cells compared to other groups. Furthermore, PCR analysis (Fig. 13) revealed significantly elevated levels of osteogenic genes in both Mg–Ca and nHAC groups. However, these levels were particularly pronounced in the Mg–Ca/nHAC group when compared to the control group. These findings showed that M2-type polarization of macrophages promotes mBMSCs' osteogenic differentiation process effectively. Western blot experiments indicated that integrin α2 and ERK1/2 protein expressions were markedly upregulated in the Mg–Ca/nHAC group while FAK and RANK protein expressions showed significant downregulation when compared to other groups (Fig. 14). These differences may be due to the distance between integrins of adhesive related particles in the nano dimension [33]. In stromal cells, activation of the integrin α2β1-FAK-ERK (MAPK) signaling pathway has been reported. Integrins are integral membrane proteins that mediate cell matrix and cell-cell adhesion. Integrins mediate cell adhesion to collagen through magnesium-dependent interactions and it can be used as messenger conversion signals to initiate downstream cascades [34,35]. Many studies have showed that Mg^{2+} played a dual role in the integrins-collagen interaction and Mg^{2+} promoted osteoblasts adhesion through integrins and activated focal adhesion kinase (FAK). FAK is a key component of the integrins-mediated signaling pathway. FAK act as a signaling molecule that transduces integrins receptor signaling through the intracellular protein cascade to participate in the adhesion process [36–39]. The RANK protein plays a crucial role in bone and immune system regulation, making it a key component in the field of bone immunity. Osteoclasts release vesicles expressing RANKL, which interact with RANK on osteoblasts. This interaction triggers RANK reverse signaling, promoting bone formation. Our previous findings demonstrated that Mg^{2+}/Type I collagen can activate the integrin α2β1-FAK-ERK1/2 pathway, thereby enhancing osteogenesis. These results are consistent with those reported in other studies. In addition, mauer et al. reported that IL-6 signalling promotes macrophage M2 polarization to reduce pronounced inflammation and insulin resistance, and identified IL-6 signalling as an important determinant of macrophage M2 polarization [40,41]. Hence, the regulation of macrophage M2-type polarization by Mg–Ca/nHAC biomaterials may involve a more intricate process that needs to be explored in the future.

The primary objective of this experiment was to investigate the impact of Mg–Ca/nHAC composites on bone repair. The findings revealed that Mg–Ca/nHAC exhibited superior osteogenic properties compared to both nHAC and Mg–Ca alloys. In future studies, we

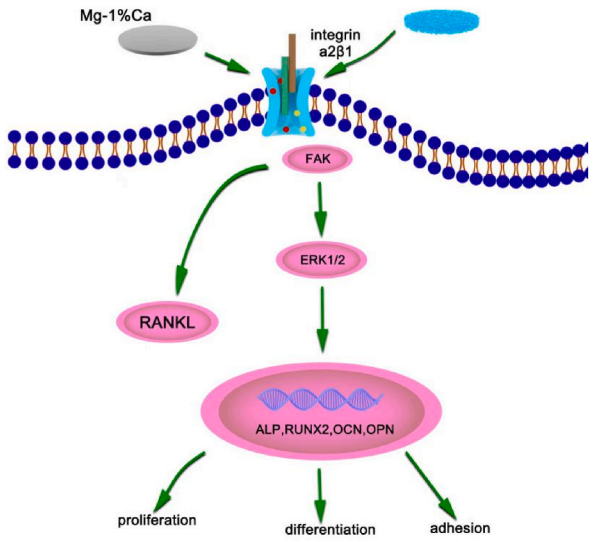

Fig. 15. Mg–Ca/nHAC biomaterials are beneficial for promoting osteogenic differentiation by promoting the integrin α2β1-FAK-ERK1/2 signaling pathway or inhibiting the osteoclast RANK signaling pathway.

can enhance the bonding method between these two materials to achieve a more tightly integrated composite structure. This material holds potential for application in load-bearing animal areas, allowing for its mechanical properties and subsequent improvement of its biological characteristics.

6. Conclusion

The objective of this study is to investigate the potential of Mg–Ca/nHAC biomaterials in promoting osteogenic differentiation of mBMSCs through modulation of the bone immune microenvironment, along with its underlying mechanism. The experiments were structured around three key aspects: osteogenic assessment, immune evaluation, and macrophage-induced osteogenic differentiation. Both macrophages and mBMSCs were cultured under various conditions, with assessments made for cell proliferation, adhesion, as well as osteogenic gene and protein expressions. In comparison to the other groups, Mg–Ca/nHAC biomaterials primarily may be induced osteogenic differentiation through M2 macrophage polarization. This effect was primarily mediated through the facilitation of the integrin α2β1-FAK-ERK1/2 signaling pathway, while concurrently inhibiting the RANK signaling pathway (as shown in Fig. 15). The findings of this study establish a theoretical foundation for the prospective utilization of Mg-based composites in bone repair tissue engineering. However, This study was limited to investigating the role of macrophage polarization in the bone immune microenvironment and its mechanisms, and the pathways were simple without exploring other relevant mechanisms. Moreover, this experiment was not further validated in vivo. Therefore, the specific role of macrophages in biomaterials research needs to be further explored.

Data availability statement

Datas can be found in xiaojing, nie (2023), "Mg–Ca/nHAC composites mediating macrophage polarization to promote bone repair", Mendeley Data, V4, https://doi.org/10.17632/7zzpr4d8tz.4.

CRediT authorship contribution statement

Xiaojing Nie: Writing – original draft, Formal analysis, Data curation, Conceptualization. **Yonghua Shi:** Methodology, Investigation. **Lei Wang:** Data curation, Conceptualization. **Wumidan Abudureheman:** Visualization, Validation. **Jingxin Yang:** Validation, Supervision, Conceptualization. **Chen Lin:** Writing – original draft, Visualization.

Declaration of competing interest

The authors declare that they have no known competing financial interests or personal relationships that could have appeared to influence the work reported in this paper.

Acknowledgments

This work was supported by Natural Science Foundation of Xinjiang Uygur Autonomous Region Project [2022D01C208] and

Natural Science Foundation of Xinjiang Uygur Autonomous Region Project [2022D01D41], Xinjiang Key Laboratory of Molecular Biology for Endemic Diseases, Xinjiang Medical University.

References

[1] Z. Chen, Y. Huai, G. Chen, S. Liu, Y. Zhang, D. Li, F. Zhao, X. Chen, W. Mao, X. Wang, C. Yin, C. Yang, X. Xu, K. Ru, X. Deng, L. Hu, Y. Li, S. Peng, G. Zhang, X. Lin, A. Qian, MiR-138-5p targets MACF1 to aggravate aging-related bone loss, Int. J. Biol. Sci. 18 (13) (2022) 4837–4852, https://doi.org/10.7150/ijbs.71411.

[2] C. Li, H. Lv, Y. Du, W. Zhu, W. Yang, X. Wang, J. Wang, W. Chen, Biologically modified implantation as therapeutic bioabsorbable materials for bone defect repair, Regen. Ther. 19 (2021) 9–23, https://doi.org/10.1016/j.reth.2021.12.004.

[3] Y. Gu, Y. Sun, S. Shujaat, A. Braem, C. Politis, R. Jacobs, 3D-printed porous Ti6Al4V scaffolds for long bone repair in animal models: a systematic review, J. Orthop. Surg. Res. 17 (1) (2022) 68, https://doi.org/10.1186/s13018-022-02960-6.

[4] K. Kato, Y. Ikeda, K. Ito, Direct determination of cross-link density and its correlation with the elastic modulus of a gel with slidable cross-links, ACS Macro Lett. 8 (6) (2019) 700–704, https://doi.org/10.1021/acsmacrolett.9b00238.

[5] T. Khodaei, E. Schmitzer, A.P. Suresh, A.P. Acharya, Immune response differences in degradable and non-degradable alloy implants, Bioact. Mater. 24 (2022) 153–170, https://doi.org/10.1016/j.bioactmat.2022.12.012.

[6] X. Zhang, Y. Gao, W. Liu, J. Liu, L. Wu, S. Xiong, J. Zhu, W. Han, J. Wang, X. Hao, S. Han, G. Huang, Frozen blastocyst embryo transfer vs. frozen cleavage-stage embryo transfer in couples with recurrent implantation failure: a cohort study, Hum. Fertil. 24 (4) (2021) 284–289, https://doi.org/10.1080/14647273.2019.1633021.

[7] Y. Zhang, J. Xu, Y.C. Ruan, M.K. Yu, M. O'Laughlin, H. Wise, D. Chen, L. Tian, D. Shi, J. Wang, S. Chen, J.Q. Feng, D.H. Chow, X. Xie, L. Zheng, L. Huang, S. Huang, K. Leung, N. Lu, L. Zhao, L. Qin, Implant-derived magnesium induces local neuronal production of CGRP to improve bone-fracture healing in rats, Nat. Med. 22 (10) (2016) 1160–1169, https://doi.org/10.1038/nm.4162.

[8] R.C. Zeng, L.Y. Cui, K. Jiang, R. Liu, B.D. Zhao, Y.F. Zheng, In vitro corrosion and cytocompatibility of a microarc oxidation coating and poly(L-lactic acid) composite coating on Mg-1Li-1Ca alloy for orthopedic implants, ACS Appl. Mater. Interfaces 8 (15) (2016) 10014–10028, https://doi.org/10.1021/acsami.6b00527.

[9] Y.F. Wang, C.Y. Wang, P. Wan, S.G. Wang, X.M. Wang, Comparison of bone regeneration in alveolar bone of dogs on mineralized collagen grafts with two composition ratios of nano-hydroxyapatite and collagen, Regenerative biomaterials 3 (1) (2016) 33–40, https://doi.org/10.1093/rb/rbv025.

[10] X. Sun, Z. Ma, X. Zhao, W. Jin, C. Zhang, J. Ma, L. Qiang, W. Wang, Q. Deng, H. Yang, J. Zhao, Q. Liang, X. Zhou, T. Li, J. Wang, Three-dimensional bioprinting of multicell-laden scaffolds containing bone morphogenic protein-4 for promoting M2 macrophage polarization and accelerating bone defect repair in diabetes mellitus, Bioact. Mater. 6 (3) (2020) 757–769, https://doi.org/10.1016/j.bioactmat.2020.08.030.

[11] Y. Sun, S. Liu, Y. Fu, X.X. Kou, D.Q. He, G.N. Wang, C.C. Fu, Y. Liu, Y.H. Zhou, Mineralized collagen regulates macrophage polarization during bone regeneration, J. Biomed. Nanotechnol. 12 (11) (2016) 2029–2040, https://doi.org/10.1166/jbn.2016.2296.

[12] X. Cui, R.T. Morales, W. Qian, H. Wang, J.P. Gagner, I. Dolgalev, D. Placantonakis, D. Zagzag, L. Cimmino, M. Snuderl, R.H.W. Lam, W. Chen, Hacking macrophage-associated immunosuppression for regulating glioblastoma angiogenesis, Biomaterials 161 (2018) 164–178, https://doi.org/10.1016/j.biomaterials.2018.01.053.

[13] X. Nie, X. Sun, C. Wang, J. Yang, Effect of magnesium ions/Type I collagen promote the biological behavior of osteoblasts and its mechanism, Regenerative biomaterials 7 (1) (2020) 53–61, https://doi.org/10.1093/rb/rbz033.

[14] T. Ono, M. Hayashi, F. Sasaki, T. Nakashima, RANKL biology: bone metabolism, the immune system, and beyond, Inflamm. Regen. 40 (2020) 2, https://doi.org/10.1186/s41232-019-0111-3.

[15] P. Makkar, S.K. Sarkar, A.R. Padalhin, B.G. Moon, Y.S. Lee, B.T. Lee, In vitro and in vivo assessment of biomedical Mg-Ca alloys for bone implant applications, J. Appl. Biomater. Funct. Mater. 16 (3) (2018) 126–136, https://doi.org/10.1177/2280800017750359.

[16] V. Sheremetyev, M. Petrzhik, Y. Zhukova, A. Kazakbiev, A. Arkhipova, M. Moisenovich, S. Prokoshkin, V. Brailovski, Structural, physical, chemical, and biological surface characterization of thermomechanically treated Ti-Nb-based alloys for bone implants, J. Biomed. Mater. Res. B Appl. Biomater. 108 (3) (2020) 647–662, https://doi.org/10.1002/jbm.b.34419.

[17] R. Gu, J. Shen, Q. Hao, J. Wang, D. Li, L. Hu, H. Chen, Harnessing superhydrophobic coatings for enhancing the surface corrosion resistance of magnesium alloys, J. Mater. Chem. B 9 (48) (2021) 9893–9899, https://doi.org/10.1039/d1tb01974k.

[18] P. Holweg, V. Herber, M. Ornig, G. Hohenberger, N. Donohue, P. Puchwein, A. Leithner, F. Seibert, A lean bioabsorbable magnesium-zinc-calcium alloy ZX00 used for operative treatment of medial malleolus fractures: early clinical results of a prospective non-randomized first in man study, Bone Joint Res. 9 (8) (2020) 477–483, https://doi.org/10.1302/2046-3758.98.BJR-2020-0017.R2.

[19] H.S. Han, I. Jun, H.K. Seok, K.S. Lee, K. Lee, F. Witte, D. Mantovani, Y.C. Kim, S. Glyn-Jones, J.R. Edwards, Biodegradable magnesium alloys promote angio-osteogenesis to enhance bone repair, Adv. Sci. 7 (15) (2020) 2000800, https://doi.org/10.1002/advs.202000800.

[20] N.G. Grün, P. Holweg, S. Tangl, J. Eichler, L. Berger, J.J.J.P. van den Beucken, J.F. Löffler, T. Klestil, A.M. Weinberg, Comparison of a resorbable magnesium implant in small and large growing-animal models, Acta Biomater. 78 (2018) 378–386, https://doi.org/10.1016/j.actbio.2018.07.044.

[21] A. Terashima, H. Takayanagi, Overview of osteoimmunology, Calcif. Tissue Int. 102 (5) (2018) 503–511, https://doi.org/10.1007/s00223-018-0417-1.

[22] A. Limmer, D.C. Wirtz, Osteoimmunology: Influence of the Immune System on Bone Regeneration and Consumption. Osteoimmunologie – immunologische Einflüsse auf den Knochenauf- und -abbau, Zeitschrift Orthopadie Unfallchirurgie 155 (3) (2017) 273–280, https://doi.org/10.1055/s-0043-100100.

[23] Y.P. Mu, Q.H. Huang, J.L. Zhu, S.Y. Zheng, F.R. Yan, X.L. Zhuang, J.S.K. Sham, M.J. Lin, Magnesium attenuates endothelin-1-induced vasoreactivity and enhances vasodilatation in mouse pulmonary arteries: modulation by chronic hypoxic pulmonary hypertension, Exp. Physiol. 103 (4) (2018) 604–616, https://doi.org/10.1113/EP086655.

[24] A.E. Haggerty, I. Maldonado-Lasunción, M. Oudega, Biomaterials for revascularization and immunomodulation after spinal cord injury, Biomed. Mater. (Bristol, U. K.) 13 (4) (2018) 044105, https://doi.org/10.1088/1748-605X/aaa9d8.

[25] L. Batoon, S.M. Millard, M.E. Wullschleger, C. Preda, A.C. Wu, S. Kaur, H.W. Tseng, D.A. Hume, J.P. Levesque, L.J. Raggatt, A.R. Pettit, CD169^{+} macrophages are critical for osteoblast maintenance and promote intramembranous and endochondral ossification during bone repair, Biomaterials 196 (2019) 51–66, https://doi.org/10.1016/j.biomaterials.2017.10.033.

[26] M.D. Costantino, A. Schuster, H. Helmholz, A. Meyer-Rachner, R. Willumeit-Römer, B.J.C. Luthringer-Feyerabend, Inflammatory response to magnesium-based biodegradable implant materials, Acta Biomater. 101 (2020) 598–608, https://doi.org/10.1016/j.actbio.2019.10.014.

[27] M. Rahmati, S. Stötzel, T.E. Khassawna, K. Iskhahova, D.C. Florian Wieland, B. Zeller Plumhoff, H.J. Haugen, Early osteoimmunomodulatory effects of magnesium-calcium-zinc alloys, J. Tissue Eng. 12 (2021) 20417314211047100, https://doi.org/10.1177/20417314211047100.

[28] J. Wang, X.Y. Ma, Y.F. Feng, Z.S. Ma, T.C. Ma, Y. Zhang, X. Li, L. Wang, W. Lei, Magnesium ions promote the biological behaviour of rat calvarial osteoblasts by activating the PI3K/Akt signalling pathway, Biol. Trace Elem. Res. 179 (2) (2017) 284–293, https://doi.org/10.1007/s12011-017-0948-8.

[29] A. Burmester, R. Willumeit-Römer, F. Feyerabend, Behavior of bone cells in contact with magnesium implant material, J. Biomed. Mater. Res. B Appl. Biomater. 105 (1) (2017) 165–179, https://doi.org/10.1002/jbm.b.33542.

[30] X. Zheng, L. Chen, J. Tan, J. Miao, X. Liu, T. Yang, Z. Ding, Effect of micro/nano-sheet array structures on the osteo-immunomodulation of macrophages, Regenerative biomaterials 9 (2022) rbac075, https://doi.org/10.1093/rb/rbac075.

[31] R. Lv, Q. Bao, Y. Li, Regulation of M1-type and M2-type macrophage polarization in RAW264.7 cells by Galectin-9, Mol. Med. Rep. 16 (6) (2017) 9111–9119, https://doi.org/10.3892/mmr.2017.7719.

[32] L. Wu, K. Chen, J. Xiao, J. Xin, L. Zhang, X. Li, L. Li, J. Si, L. Wang, K. Ma, Angiotensin II induces RAW264.7 macrophage polarization to the M1-type through the connexin 43/NF-κB pathway, Mol. Med. Rep. 21 (5) (2020) 2103–2112, https://doi.org/10.3892/mmr.2020.11023.

[33] C. Arous, B. Wehrle-Haller, Role and impact of the extracellular matrix on integrin-mediated pancreatic β-cell functions, Biol. Cell. 109 (6) (2017) 223–237, https://doi.org/10.1111/boc.201600076.
[34] J.A. Eble, M. McDougall, G.L. Orriss, S. Niland, B. Johanningmeier, G. Pohlentz, M. Meier, S. Karrasch, M.I. Estevão-Costa, A. Martins Lima, J. Stetefeld, Dramatic and concerted conformational changes enable rhodocetin to block α2β1 integrin selectively, PLoS Biol. 15 (7) (2017) e2001492, https://doi.org/10.1371/journal.pbio.2001492.
[35] D.Y. Yuh, T. Maekawa, X. Li, T. Kajikawa, K. Bdeir, T. Chavakis, G. Hajishengallis, The secreted protein DEL-1 activates a β3 integrin-FAK-ERK1/2-RUNX2 pathway and promotes osteogenic differentiation and bone regeneration, J. Biol. Chem. 295 (21) (2020) 7261–7273, https://doi.org/10.1074/jbc.RA120.013024.
[36] C.O. McAtee, C. Booth, C. Elowsky, L. Zhao, J. Payne, T. Fangman, S. Caplan, M.D. Henry, M.A. Simpson, Prostate tumor cell exosomes containing hyaluronidase Hyal1 stimulate prostate stromal cell motility by engagement of FAK-mediated integrin signaling, Matrix Biol. 78–79 (2019) 165–179, https://doi.org/10.1016/j.matbio.2018.05.002.
[37] R. Jahan, M.A. Macha, S. Rachagani, S. Das, L.M. Smith, S. Kaur, S.K. Batra, Axed MUC4 (MUC4/X) aggravates pancreatic malignant phenotype by activating integrin-β1/FAK/ERK pathway, Biochim. Biophys. Acta, Mol. Basis Dis. 1864 (8) (2018) 2538–2549, https://doi.org/10.1016/j.bbadis.2018.05.008.
[38] Y. Zhao, X. Zhang, X. Zhang, G. Shen, W. Li, Q. Wang, Integrinβ1/FAK/ERK signalling pathway is essential for Chinese mitten crab Eriocheir sinensis hemocyte survival, Fish Shellfish Immunol. 132 (2023) 108473, https://doi.org/10.1016/j.fsi.2022.108473.
[39] B. Li, P. Wang, J. Jiao, H. Wei, W. Xu, P. Zhou, Roles of the RANKL-RANK Axis in immunity-implications for pathogenesis and treatment of bone metastasis, Front. Immunol. 13 (2022) 824117, https://doi.org/10.3389/fimmu.2022.824117.
[40] H. Han, G. Ding, S. Wang, J. Meng, Y. Lv, W. Yang, H. Zhang, X. Wen, W. Zhao, Long non-coding RNA LOC339059 attenuates IL-6/STAT3-signaling-mediated PDL1 expression and macrophage M2 polarization by interacting with c-Myc in gastric cancer, Cancers 15 (22) (2023) 5313, https://doi.org/10.3390/cancers15225313.
[41] Z. Chen, H. Wu, R. Shi, W. Fan, J. Zhang, W. Su, Y. Wang, P. Li, miRNAomics analysis reveals the promoting effects of cigarette smoke extract-treated Beas-2B-derived exosomes on macrophage polarization, Biochem. Biophys. Res. Commun. 572 (2021) 157–163, https://doi.org/10.1016/j.bbrc.2021.07.093.